



29 **ABSTRACT**

30 Asphaltenes were obtained from a Brazilian vacuum residue (VR) by precipitation  
31 with different ratios of *n*-heptane/VR to have three subfractions of the asphaltene. The  
32 behavior of these different subfractions in the stability of water-in-oil (W/O)  
33 emulsions was evaluated. The whole asphaltene subfraction (AH) was obtained by  
34 addition 40:1 volumes of *n*-heptane/VR followed by filtration. Two different  
35 asphaltene subfractions (A4 and A10) were obtained by precipitation with a  
36 successive increasing *n*-heptane/VR ratio, from 4:1 and 10:1, respectively. The  
37 properties of these precipitated subfractions of asphaltenes were analyzed by  
38 atmospheric pressure photoionization (APPI) coupled to Fourier transform ion  
39 cyclotron resonance mass spectrometry (FT-ICR MS) in a positive-ion mode,  
40 ultraviolet-visible (UV-Vis) spectroscopy and nuclear magnetic resonance (NMR)  
41 spectroscopy. The FT-ICR MS results showed that the 4:1 subfraction (A4) exhibited  
42 a profile with higher heteroatoms components, high polarity and molecular weight  
43 distribution ( $M_w$ ). An inverse correlation was observed with respect to aromaticity  
44 degree and solubility in heptane/toluene solutions (onset point). The subfractions AH  
45 and A10 were more aromatic than the subfraction A4, being the results confirmed by  
46  $^1\text{H}$  NMR analysis. Besides, asphaltenes subfractions promoted a great stability in the  
47 produced emulsions. The droplet size distribution and bottle test showed similar  
48 results for emulsion stability formed with the three different subfractions. After  
49 application of centrifugal forces, the formation of a dense packed layer emulsion was  
50 observed containing approximately 85% water that remained stable for 2 weeks.

51

52 **Keywords:** water-in-oil emulsion; asphaltene fractionation; dense packed layer;  
53 asphaltene onset; FT-ICRMS analysis.

54        **1. Introduction**

55            Asphaltenes are a complex mixtures of molecules, which consists of  
56 condensed aromatic rings with aliphatic side chains, heteroatoms such as N, O, S and  
57 metals such as Fe and V. (Dudásova *et al.*, 2008; Speight, 2007). They are typically  
58 defined as the nonvolatile oil fraction, insoluble in n-alkanes, such as heptane, and  
59 soluble in aromatics solvents, such as toluene (Dudásova *et al.*, 2008; Sjoblom *et al.*,  
60 2003; Speight, 2007). Asphaltenes have propensity to aggregate, and their tendency to  
61 self-associate depends on the aromaticity of the solvent, the thermodynamic  
62 conditions, such as temperature and/or pressure and the presence of co-solutes such as  
63 resins. Generally, their aggregate size increases as a function of the increase of the  
64 aliphatic solvent volume or due to the reduction of the pressure (Sjoblom *et al.*, 2003).  
65 Asphaltenes are responsible for some problems in the petroleum industry, including  
66 precipitation and deposition during crude oil production, processing and transport  
67 (Sjoblom *et al.*, 2015).

68            In the crude oil industry, water-in-oil (W/O) emulsions can be found in almost  
69 all processes of production and oil recovery. These emulsions increase the viscosity of  
70 the crude oil, and affect the flow operations, leading to enormous economic losses  
71 during the recovery, treatment, and transportation of crude oil. W/O emulsions  
72 are stabilized by several surface-active species usually found in the crude oil such as  
73 resins, asphaltenes, fine solids, organic acids and bases. Asphaltenes are commonly  
74 identified as compounds which have a higher tendency to migrate to the W/O  
75 interface introducing a barrier that prevents the droplets from coalescing, yielding  
76 high emulsion stability (Samaniuk *et al.*, 2015; Yang *et al.*, 2007).

77            A variety of standards procedures exist to precipitate asphaltenes from crude  
78 oil. The conventional method is first to precipitate the whole asphaltene fraction from

79 crude oil by adding excess of the *n*-heptane or *n*-pentane to crude oil (40 volumes of  
80 solvent to 1 volume of oil). Due to asphaltene complexity, whole asphaltene is often  
81 subfractionated aiming at a fine identification of its behavior. This fractionation  
82 process can be accomplished by different methods, including adsorption on solids  
83 (Nascimento *et al.*, 2016) and treatments with different solvents (Fossen *et al.*, 2007b;  
84 Speight, 2007; Yang *et al.*, 2004). Produced subfractions of asphaltenes may have  
85 different functionality, solubility and composition. The chemical and structural  
86 characterization of asphaltenes and subfractions are the key to understand their  
87 properties and their behavior (Castillo *et al.*, 2015; Nalwaya *et al.*, 1999; Trejo *et al.*,  
88 2004).

89 Different analytical methods have been used to characterize asphaltenes and  
90 their subfractions, such as nuclear magnetic resonance (NMR) spectroscopy (Pereira  
91 *et al.*, 2014b), infrared (IR) spectroscopy (Rogel *et al.*, 2015), vapor-pressure  
92 osmometry (VPO) (Acevedo *et al.*, 2010) and ultraviolet-visible (UV-vis)  
93 spectroscopy (Nascimento *et al.*, 2016). Currently, Fourier transform ion cyclotron  
94 resonance mass spectrometry (FT-ICR MS) is one of the few techniques that enable  
95 the analysis at the molecular level of complex mixtures such as asphaltenes and  
96 petroleum (Cho *et al.*, 2012). The ultra-high resolution and mass accuracy of the FT-  
97 ICR MScan define a unique elemental composition ( $C_cH_hN_nO_oS_s$ ) and double bond  
98 equivalent (DBE), facilitating material classification by heteroatom content and  
99 degree of aromaticity (Pereira *et al.*, 2014b).

100 Pereira *et al.*(2014b) analyzed Brazilian asphaltene sample using different  
101 ionization sources, such as electrospray ionization (ESI), atmospheric pressure  
102 chemical ionization (APCI), atmospheric pressure photoionization (APPI), laser  
103 desorption/ionization (LDI) and matrix-assisted laser desorption/ionization (MALDI)

104 to understanding the effects caused by the ionization parameters during the  
105 asphaltenes analysis. It was demonstrated that each source acquired a distinct  
106 chemical profile of compounds classes, revealing specific singularities of the sample.  
107 In addition to that, it was demonstrated that APCI and APPI accessed a wide range of  
108 compound classes, DBEs and carbon number distributions within the evaluated  
109 ionization sources (Pereira *et al.*, 2014b).

110 In these study, we precipitated three asphaltenes fractions using a gradually  
111 increase of *n*-heptane/VR ratio (40:1, 4:1 and 10:1). The asphaltene fractions were  
112 characterized using APPI(+)-FT-ICR MS. For each sample, relative abundance  
113 distributions of the heteroatom class, van Krevelen diagram and the graphical DBE  
114 *versus* carbon number images were generated. Based on the asphaltenes subfractions  
115 obtained by different toluene/*n*-heptane ratios, it was possible to determinate the  
116 solubility profile. The ability to stabilize W/O emulsion for the three different  
117 subfractions produced was analyzed through bottle test and droplet size distribution,  
118 and the results compared with the chemical properties of each subfraction.

119

## 120 **2. Experimental**

### 121 **2.1 Materials**

122 The vacuum residue (VR) used in this study was supplied by Petrobras  
123 (Presidente Getúlio Vargas Refinery - REPAR) and consists of an asphaltic residue  
124 formed during the vacuum distillation of a blend of 10 different crude oils. The *n*-  
125 heptane solvent applied in the asphaltene extraction (purity > 99.5%) was supplied by  
126 Sigma-Aldrich Chemicals Brazil (Rio de Janeiro-Brazil). Toluene (>98%) used in the  
127 APPI(+)-FT-ICR MS analysis was purchased by Vetec<sup>®</sup> Química Fina Ltda (Rio de  
128 Janeiro-Brazil). All reagents were used as received.

129

## 130 2.2 Asphaltenes precipitation

131 | The VR was submitted to an extraction procedure where whole asphaltene  
132 | was precipitated by addition of *n*-heptane in a 40:1 solvent-to-VR (cm<sup>3</sup>/g) ratio.  
133 | Initially, VR was heated to 140<sup>0</sup>C for at least 1hour and then stirred to provide  
134 | homogenization. Subsequently, 4g of the VR were dissolved in 160 mL of *n*-heptane.  
135 | This mixture was left on magnetic stirrer for 24 hours. After, the precipitate was  
136 | recovered by vacuum filtration through a 0.45 μm filter (Unifil<sup>®</sup>) and washed with an  
137 | excess of *n*-heptane, to remove the remaining soluble material. Then, the whole  
138 | asphaltene, named AH, was dried in a desiccator at room temperature until the mass  
139 | was invariant. The yield of this AH subfraction was 11.2 wt% (± 0.2).

140 | Two other subfractions were obtained based in a procedure described by  
141 | Fossen et al. (2007b), where asphaltenes were precipitated with a successive increase  
142 | of *n*-heptane. Briefly, the first subfraction was obtained using a ratio of 4:1 *n*-  
143 | heptane/VR (wt/wt). This mixture was shaken for 24 hours and the precipitated  
144 | material, was then separated by vacuum filtration through a 0.45 μm filter and  
145 | designated as A4, with a yield of 6.8wt% (± 0.4). The subfraction A10 was  
146 | precipitated adding *n*-heptane to the supernatant of the first step and the *n*-heptane/VR  
147 | ratio was adjusted to 10:1. This mixture was shaken for 24 hours and the precipitated  
148 | material was then separated by vacuum filtration through a 0.45 μm filter, with a yield  
149 | of 3.1 wt% (± 0.2). Both A4 and A10 were washed with an excess of hot *n*-heptane.  
150 | The subfractions were dried in a desiccator at room temperature until the mass was  
151 | invariant.

152

### 153 **2.3 <sup>1</sup>H nuclear magnetic resonance (<sup>1</sup>H NMR)**

154 The degree of aromaticity of the VR and their asphaltenes subfractions were  
155 obtained by <sup>1</sup>H NMR analysis. <sup>1</sup>H NMR experiments were performed on a Varian  
156 VNMRS 400 spectrometer; operating at 9.4 T using 5 mm broadband <sup>1</sup>H/X/D probe.  
157 All experiments were performed at 25 °C. The aromatic hydrogen content (%) was  
158 determined through the integration of areas from 9.0 to 6.0 ppm regions, and aliphatic  
159 hydrogen through the integration of areas 4.0 to 0.0 ppm regions (Da Silva de  
160 Oliveira et al., 2014; Nascimento et al., 2016).

161

### 162 **2.4 APPI (+)-FT-ICR MS**

163 VR, AH and the subfractions (A4 and A10) were characterized by FT-ICR  
164 MS. FT-ICR MS analyses were performed using a 9.4 T Q-FT-ICR MS hybrid  
165 (Solarix, Bruker Daltonics, Bremen, Germany) equipped with commercially  
166 available APPI source, set to operate over a mass region of  $m/z$  200-1000. FT-ICR  
167 mass spectra of VR, AH and subfractions (A4 and A10) were acquired using positive-  
168 ion ionization mode for APPI, APPI(+). Briefly, all samples were diluted to  
169 | proximally 1 to 2 mg·mL<sup>-1</sup> in toluene. The solutions were then sonicated for 5 min to  
170 | ensure solubility. The resulting solutions were directly infused into the ionization  
171 | source at 10 μL·min<sup>-1</sup>.

172 The APPI(+) source conditions were as follows: nebulizer gas pressure of  
173 2.0 bar, capillary voltage of 2-3 kV, transfer capillary temperature of 250 °C and  
174 Krypton photoionization lamp. Ions were accumulated in a hexapole for 3.0 s and  
175 transferred to the ICR cell through the multipole ion guide system (another hexapole).  
176 Each spectrum was acquired using 200 scans of time-domain transient signals in 4  
177 mega-point time domain data sets. The front and back trapping voltages in the ICR

178 cell were +0.85V for APPI(+). All mass spectra were externally calibrated using a  
179 NaTFA solution ( $m/z$  from 200 to 1200) after they were internally recalibrated using a  
180 set of the most abundant homologous alkylated compounds for each sample (Pereira  
181 *et al.*, 2014a; Pereira *et al.*, 2014b).

182 The mass spectra were acquired and processed using a custom algorithm  
183 developed specifically for petroleum data processing, Composer *software* (Sierra  
184 Analytics, Modesto, CA, USA). The heteroatomic containing compounds, Van  
185 Krevelen (1950) diagrams and DBE versus carbon number (CN) were constructed  
186 (Kendrick, 1963). DBEs represent the number of rings plus the double bonds  
187 involving carbon, and can be calculated by the following **equation 1**:

$$188 \quad \text{DBE} = c - \frac{h}{2} + \frac{n}{2} + 1 \quad (\text{eq. 1})$$

189 Where  $c$ ,  $h$ , and  $n$  are the numbers of carbon, hydrogen, and nitrogen atoms,  
190 respectively, in the molecular formula.

191

## 192 **2.5 Onset of Precipitation of asphaltenes subfractions in Heptane/Toluene** 193 **mixtures**

194 A serie of asphaltene subfraction/toluene solutions with a concentration of 5%  
195 wt/v were prepared. The solutions were homogenized in a shaker for 24 hours and left  
196 on a sonic bath for 15 min. For each solution, a known amount was sampled (1mL)  
197 and mixed with *n*-heptane/toluene solutions (9 mL heptol) with different heptane to  
198 toluene ratios (0:100, 10:90, 20:80, 30: 70, 40:60, 50:50, 60:40, 70:30, 80:20 and  
199 90:10 heptol), reaching a final concentration of asphaltene in each centrifuge tube of  
200 0.5wt%. These samples were shaken for 24 hours, followed by centrifugation at 3000  
201 rpm for 30 min. The onset of precipitation of asphaltenes subfractions was obtained  
202 using a Varian Cary 50 ultraviolet visible spectrometer at wavelength of 875nm



203 (Loureiro *et al.*, 2015).

204

## 205 **2.6 Emulsion stability test**

206 Model emulsions using asphaltenes subfractions dispersed in heptol were  
207 prepared to examine the influence of these different subfractions in the stability of  
208 emulsions. Mixtures of 60:40 heptol containing 0.5% of asphaltene subfraction (wt/v)  
209 were used as model oils. The aqueous phase was prepared with 50gL<sup>-1</sup>NaCl in  
210 deionized water. Equal volume of oil phase and aqueous phase were emulsified using  
211 Polytron homogenizer (PT 3100D) at 18000 rpm for 3 min. The emulsions obtained  
212 were placed in 15 mL centrifuge tubes and monitored using the bottle test method for  
213 24 h at room temperature (22 °C ± 2 °C). After, the emulsions were then centrifuged  
214 at 5000 rpm for 15 min to separate the free oil phase from the remaining emulsion  
215 phase, with this latter one looking dense and opaque, suggesting the formation of a  
216 dense packed layer (DPL). Aliquots of the free oil phase were sent for asphaltene  
217 content characterization as analyzed by UV-VIS spectrum and the emulsified  
218 phase(the so-called DPL) was analyzed at the Karl Fischer.

219

## 220 **2.7 Emulsion characterizations**

221 Emulsion properties such as droplet size distribution (DSD), water content and  
222 asphaltene content were characterized before and after each stability test. The droplet  
223 size distribution was measured by optical microscopy analysis using an inverter  
224 | microscope Zeiss Observer D1 (Zeiss Vision GmbH, Germany) set to 1600X and a  
225 camera attached to the microscope was used to capture images. The images were  
226 processed in Axio Vision software. The stable emulsions were analyzed at room  
227 temperature after 24 h under the influence of gravity. The DSD analysis was

228 performed on three different micrographs, and at least 300 droplets were counted for  
229 obtaining the average droplet diameter.

230 A Karl Fisher volumetric titrator KEM-EBU, model KF-610 - Automatic  
231 Potentiometric Titrator AT-510 was used to measure the water content in the  
232 emulsions formed after centrifugation process, according to ASTM D 1744. Water  
233 content was reported as a weight percentage.

234 Asphaltene contents in the free oil phase obtained after centrifugation were  
235 analyzed by UV spectroscopy performed with the spectrophotometer Shimadzu  
236 Corporation in a wavelength of 336 nm (Kelesogluet al., 2014). Prior to measurement,  
237 calibration curves were constructed by preparing a series of asphaltenes in 9 ml of  
238 toluene and 1 ml of 60:40 heptol solutions, with concentration ranging from 0.01 g.L<sup>-1</sup>  
239 to 0.06 g.L<sup>-1</sup>. The free oil phase was then diluted in toluene to match the calibration  
240 curve range. The concentration of asphaltenes was then calculated by evaluating the  
241 absorbance at  $\lambda= 336$  nm.

242

### 243 **3. Results and discussion**

#### 244 **3.1 <sup>1</sup>H NMR analysis**

245 The VR and all subfractions of asphaltenes (AH, A4 and A10) were  
246 characterized by <sup>1</sup>H NMR spectroscopy, where the results are described in **Table 1**.  
247 The NMR results show lower aromatic hydrogen content (H<sub>ar</sub>) for the VR sample,  
248 whereas for the asphaltenes subfractions, higher and similar H<sub>ar</sub> values are reported.  
249 Note that a slight increase in the values of H<sub>ar</sub> is observed from subfraction A4 to  
250 A10, with this latter exhibiting a more aromatic profile.

251

252

253 **Table 1.** <sup>1</sup>H NMR analysis of vacuum residue (VR) and its asphaltenes subfractions.

Samples	Chemical shift (ppm)	
	(%mol) H <sub>ar</sub> (6.0-9.0)	(%mol) H <sub>alk</sub> (0.5 -4.0)
VR	5.9	94.1
AH	10.4	89.6
A4	10.3	89.7
A10	10.6	89.4

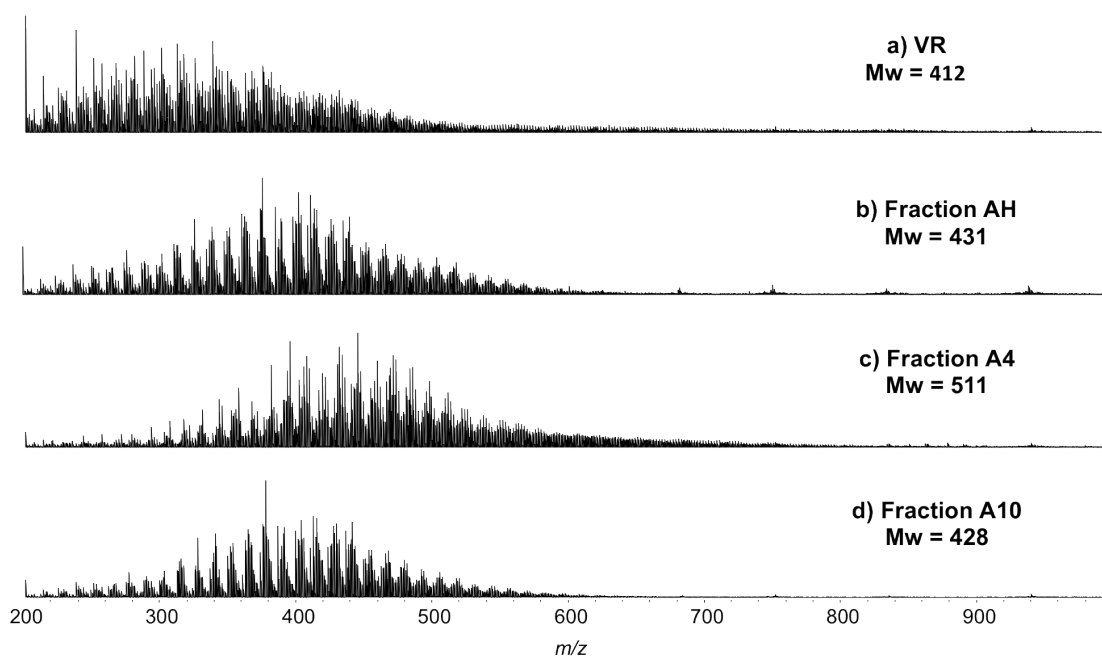
254

### 255 3.2 APPI(+)-FT-ICR MS

256 **Figure 1** shows the APPI(+)-FT-ICR mass spectra of the VR sample and its  
257 asphaltenes subfractions (AH, A4 and A10). The FT-ICR mass spectra show broad  
258 band profiles from  $m/z$  200-650, with average molar distribution ( $M_w$ ) centered at  
259 approximately  $m/z$  412, 431, 511 and 428 for VR, AH, A4 and A10, respectively.  $M_w$   
260 values increases in the following order for the subfractions: A10 < AH < A4. For the  
261 subfraction AH (**Figure 1b**), a broader range mass profile and a shift toward larger  
262  $m/z$  values is observed when compared to sample VR. For the other two subfractions  
263 (A4 and A10) (**Figure 1, c and d**) a shift toward larger  $m/z$  values are also observed.  
264 The higher  $M_w$  presented by A4 subfraction (**Figure 1c**) could be due to higher  
265 proportion of VR added to solvent (ratio of 4:1 *n*-heptane/ RV (wt/wt)). This favors at  
266 a higher abundance of heavier components that were accumulated in precipitated  
267 subfraction. Other studies have reported  $M_w$  values similar to the ones showed in  
268 work. Nascimento *et al.* (2016) precipitated, by adsorption onto silica particles, three  
269 different subfractions from Brazilian light oil and analyzed by APPI(+)-FT-ICR MS.  
270 The subfractions showed  $M_w$  values lower than 600 Da. Pereira *at el.* (2014a)  
271 characterized asphaltenes precipitated from three different Brazilian crude oil in *n*-  
272 heptane using APPI(+)-FT-ICR MS. The three different subfractions also showed  
273  $M_w < 600$  Da.

274

275

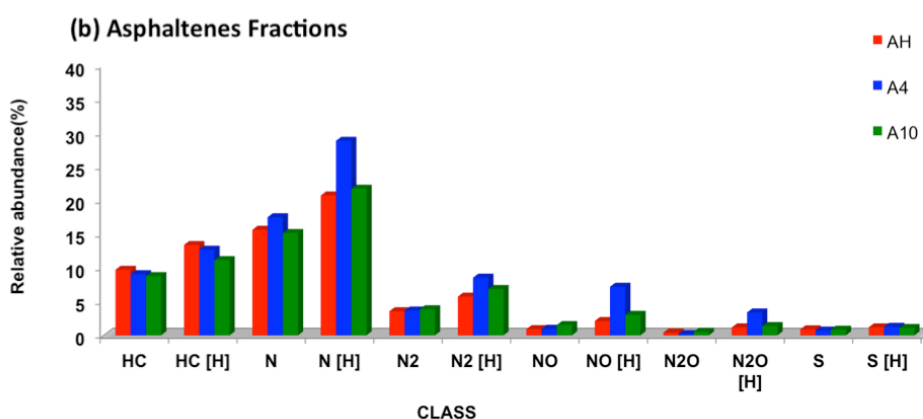
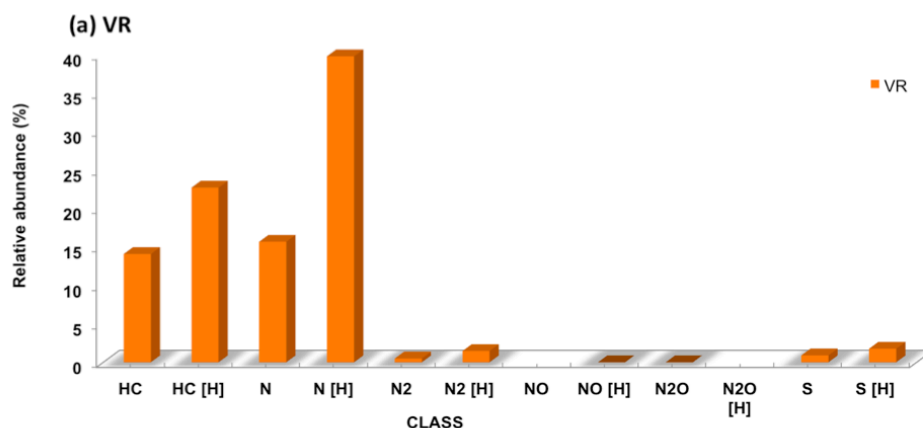


276

277 **Figure 1.** APPI(+)-FT-ICR mass spectra of vacuum residue and its asphaltene  
278 subfractions.

279

280 **Figure 2** shows the polar and nonpolar compounds class distribution of VR  
281 sample (**Figure 2a**) and its asphaltene subfractions (**Figure 2b**). For the VR sample  
282 (**Figure 2a**), a higher abundance of N[H] compounds is observed, following by  
283 HC[H], N, and HC classes. On the other hand, asphaltene subfractions (**Figure 2b**)  
284 exhibit a higher variety of highly polar compounds classes (N<sub>2</sub>, N<sub>2</sub>[H], NO[H] and  
285 NO<sub>2</sub>[H]), which in turn represents a behavior expected for a typical asphaltene  
286 sample. Among the asphaltene subfractions, the sample A4 presents the highest  
287 concentration of polar compound species, thus suggesting that this subfraction is the  
288 most polar.



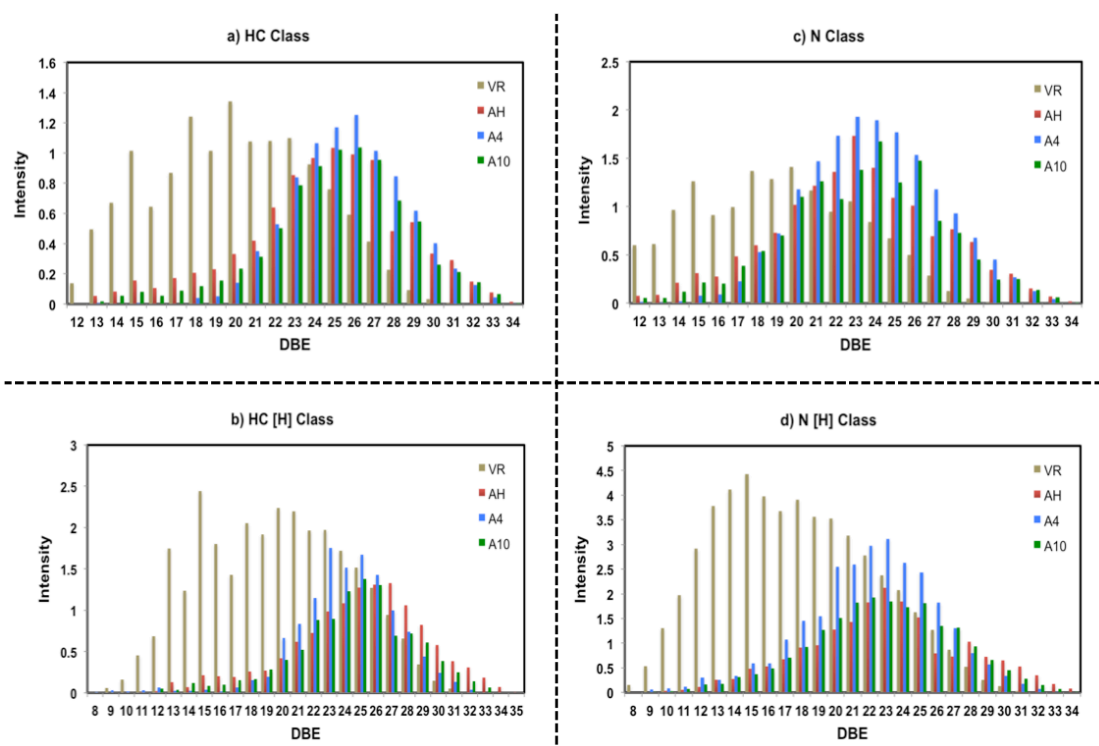
289

290 **Figure 2.** Class distribution generated from APPI(+)-FT-ICR MS data for (a) VR  
 291 sample and its (b) asphaltene subfractions.

292

293 The DBE relative abundance distributions of HC, HC[H], N and N[H] classes  
 294 for the VR sample and its asphaltene subfractions (AH, A4 and A10) are shown in  
 295 **Figure 3(a-d)**. DBE distribution for asphaltene subfractions shows a progressive  
 296 shifting to higher DBE value when compared to VR, as seen in **Figure 3a-d**.  
 297 Furthermore, DBE distribution ranges from 12 to 34 for all asphaltene subfractions  
 298 and shows a maximum abundance of DBE centered on average at 26 for HC and  
 299 HC[H] classes and 23 for N and N[H] classes. For the protonated classes (HC [H] and  
 300 N[H]) (**Figure 3b** and **d**), it is more evident that the subfraction A4 presents a less

301 aromatic profile than other subfractions (AH and A10), corroborating with the  $^1\text{H}$   
302 NMR analysis (**Table 1**).



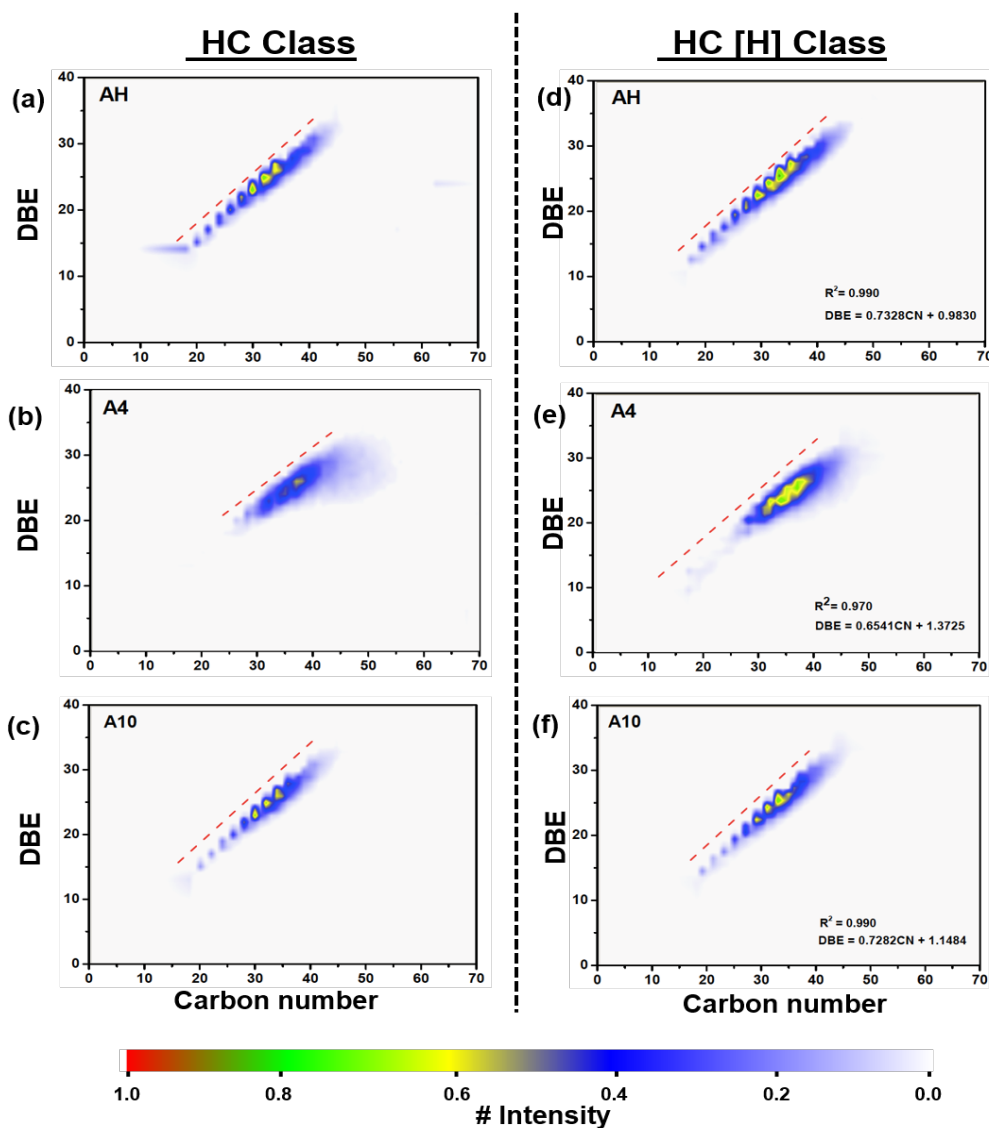
303

304 **Figure 3.** DBE relative abundance distribution for the **(a)** HC, **(b)** HC[H], **(c)** N  
305 and **(d)** N[H] classes for VR sample, and its asphaltene subfractions (AH, A4 and  
306 A10).

307 **Figures 4 and 5** show the DBE *versus* carbon number (CN) plots for the most  
308 abundance classes of radical and protonated molecules detected, HC and HC[H]  
309 classes (**Figure 4**) and N and N[H] classes (**Figure 5**), respectively. Structural  
310 interpretation is possible by the concept of planar slopes, which are defined as lines  
311 that connect maximum observed DBE values with specific carbon numbers. The  
312 slopes of these lines were calculated by linear regression, where the increase of slope  
313 of line is proportional to the increase in the  $H_{ar}$  values, giving the possibility to extract  
314 the aromaticity degree for each sample (Pereira et al., 2014a).

315 **Figure 4a-f** exposes the DBE *versus* CN for HC and HC[H] classes of  
316 subfractions AH (**4a-d**), A4 (**4b-e**) and A10 (**4c-f**). A wider polyaromatic compounds

317 distribution is observed for subfraction AH, with DBE and CN ranging from 10 to 35  
 318 and C<sub>10</sub> to C<sub>50</sub>, respectively. For subfraction A4, a shorter DBE and CN distribution is  
 319 observed (DBE = 18-32 and CN of C<sub>25</sub>-C<sub>52</sub>). The slopes decrease in the following  
 320 order: subfraction AH ~ subfraction A10 > subfraction A4, indicating that the  
 321 subfraction A4 has a higher aliphatic character compared to the other asphaltenes.



322

323 **Figure 4.** DBE *versus* carbon number plots for HC and HC[H] classes for asphaltenes  
 324 subfractions AH (a-d), A4 (b-e) and A10 (c-f).

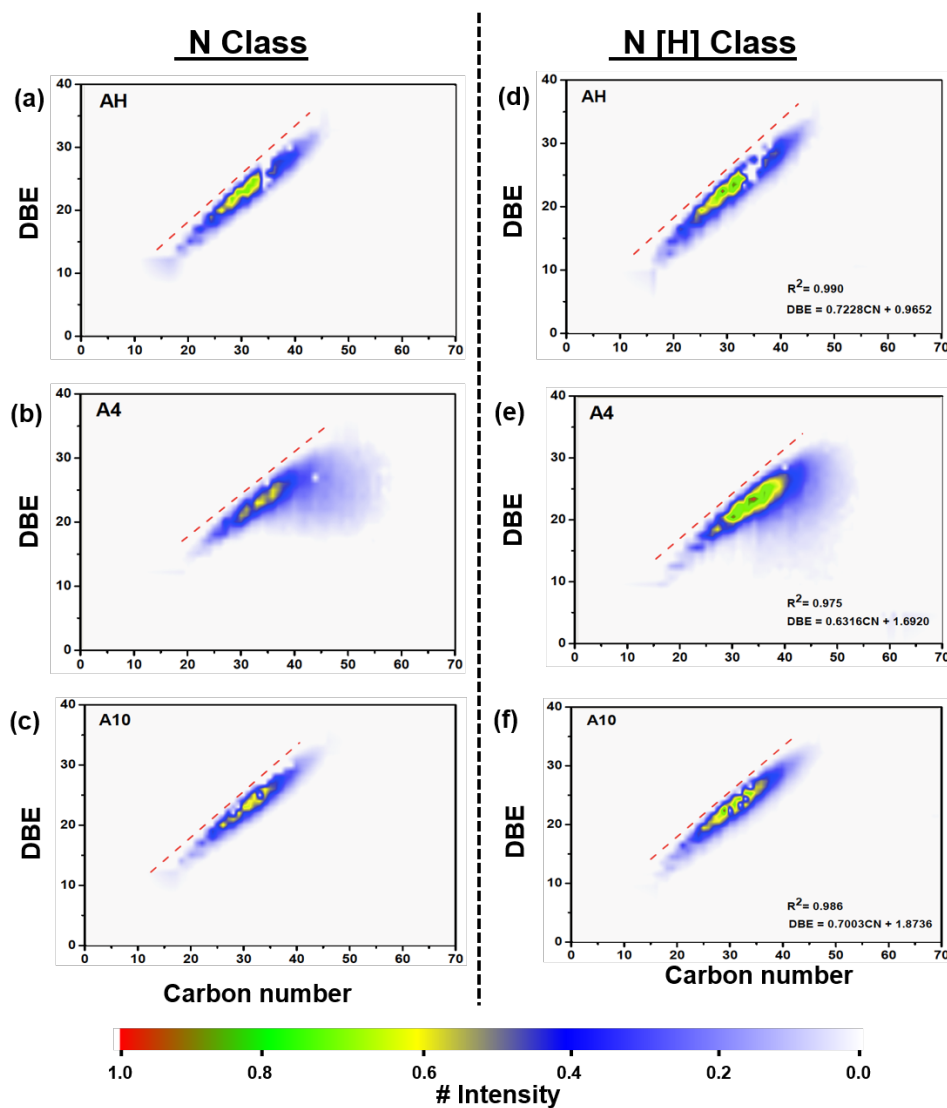
325

326

327

For the N and N[H] classes (Figure 5a-f), the asphaltene subfraction samples exhibit a higher amplitude of distribution of DBE and CN values, ranging from 10 to

328 35 and from C<sub>15</sub> to C<sub>50</sub>. Similar to **Figure 4**, an increasing of the inclination of the  
 329 planar line of DBE *versus* CN plot obeys the following order: subfraction AH  
 330 >subfraction A10 >subfraction A4. Note that a higher population of nitrogenated  
 331 compounds and low aromaticity is observed for subfraction A4, **Figures 5b-e**.



332  
 333 **Figure 5.** DBE *versus* carbon number plots for N and N[H] classes for asphaltene  
 334 subfractions (AH, A4 and A10).

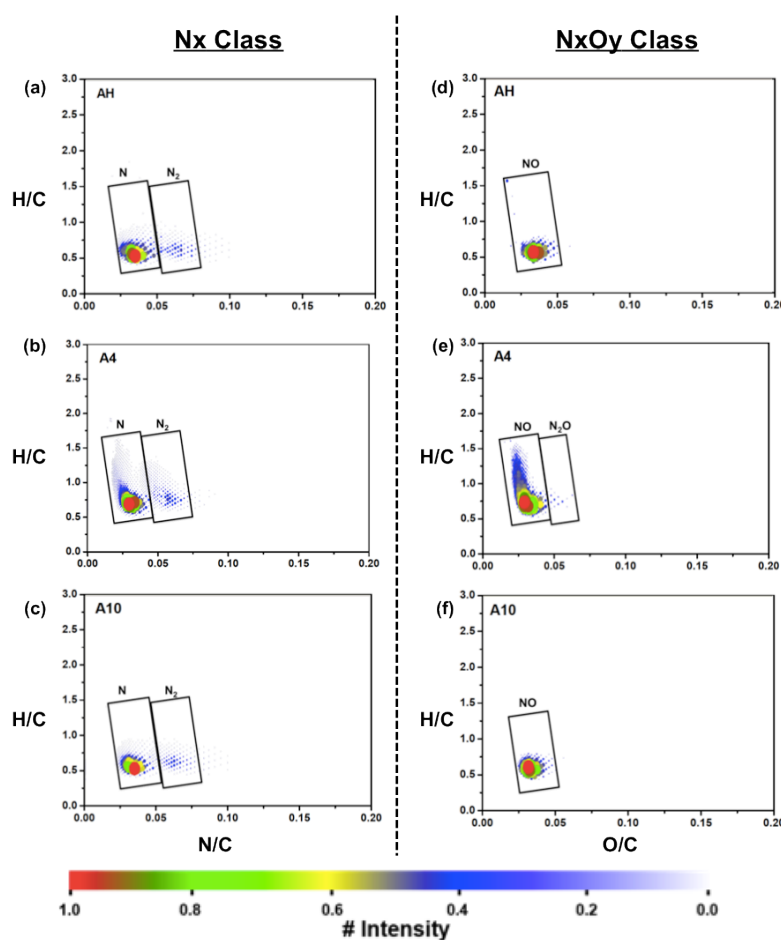
335

336 The van Krevelen diagrams consist of iso-abundance contours as function of  
 337 H/C ratio and N/C ratio for each compound containing those atoms (Klein et al.,



338 2006a). The van Krevelen allows a convenient visual separation of heteroatom class,  
339 DBE (type) and alkylation pattern (Klein et al., 2006b).

340 **Figure 6a-f** illustrates the  $N_x$  and  $N_xO_y$  profile classes of asphaltenes  
341 subfractions. The subfraction A4 (**Figure 6b**) exhibits a greater amplitude compounds  
342 at the H/C ratio varying from 0.5 to 1.7, with maximum centered at 0.7 for the  $N_x$   
343 profile classes. Whereas, the subfractions AH (**Figure 6a**) and A10 (**Figure 6c**) show  
344 a lower amplitude of compounds detected, with H/C ratio from 0.3 to 1.0, with  
345 maximum centered at 0.5. When the H/C ratio decreases, the number of rings plus  
346 double bonds increase, proving that the higher aromatic character is present in  
347 subfractions AH and A10 (Klein et al., 2006b).



348

349

350 **Figure 6.** van Krevelen diagrams for  $N_x$  and  $N_xO_y$  containing species generated from  
351 APPI(+)-FT-ICR MS data of asphaltene subfractions.

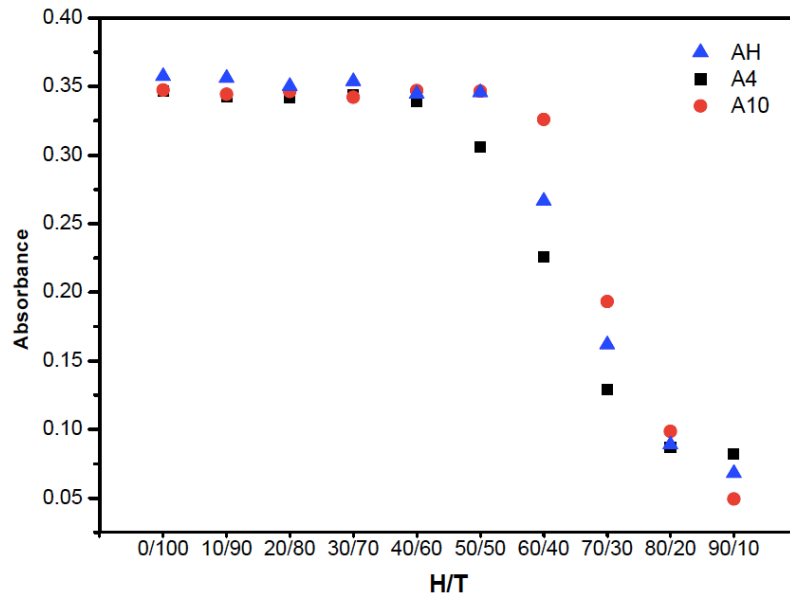
352 The  $N_xO_y$  profile classes (**Figure 6d-f**) present similar behavior in relation to  
353 data of **Figure 6a-c**. Subfraction A4 (**Figure 6e**) exhibits again greater amplitude of  
354 compounds (H/C ratio varying from 0.5 to 1.5, with maximum centered at 0,7) when  
355 compared with the other (subfractions AH and A10). The last two subfractions  
356 | (**Figure 6d and f**) show lower amplitude of  $N_xO_y$  compounds, with H/C ratio from 0.3  
357 to 0.7, with maximum centered at 0.5). Therefore, the FT-ICR MS data are in  
358 agreement with the  $^1H$  NMR analysis (**Table 1**).

359

### 360 **3.3 Asphaltene precipitation onset results**

361 The onset point was obtained through the ultraviolet-visible (UV-Vis) and the  
362 results are shown in **Figure 7**. Note that the absorbance values remain constant until  
363 the 40:60 ratio of *n*-heptane/toluene for subfraction A4 and 50:50 for subfractions AH  
364 and A10. After these ratios, it can be observed a decrease in absorbance values,  
365 indicating a reduction on asphaltene concentration in the solution. The point in which  
366 the absorbance began to decrease indicates the onset of precipitation of asphaltenes.  
367 For the subfractions AH and A10, the precipitation onset occurred in the 60:40 ratio  
368 of *n*-heptane/toluene. For the subfraction A4, the onset happened in the ratio 50:50 of  
369 *n*-heptane/toluene. These data indicate that subfraction A4 is the least soluble of all  
370 the subfractions. Spiecker *et. al.*(2003) studied the solubility of the asphaltenes  
371 fractions in the *n*-heptane/toluene mixtures to four different oils, similar results were  
372 presented, where the most polar fractions had low solubility.

373



374

375 **Figure 7.** Onset of precipitation results for asphaltene subfractions AH, A4 and A10  
 376 into heptol.

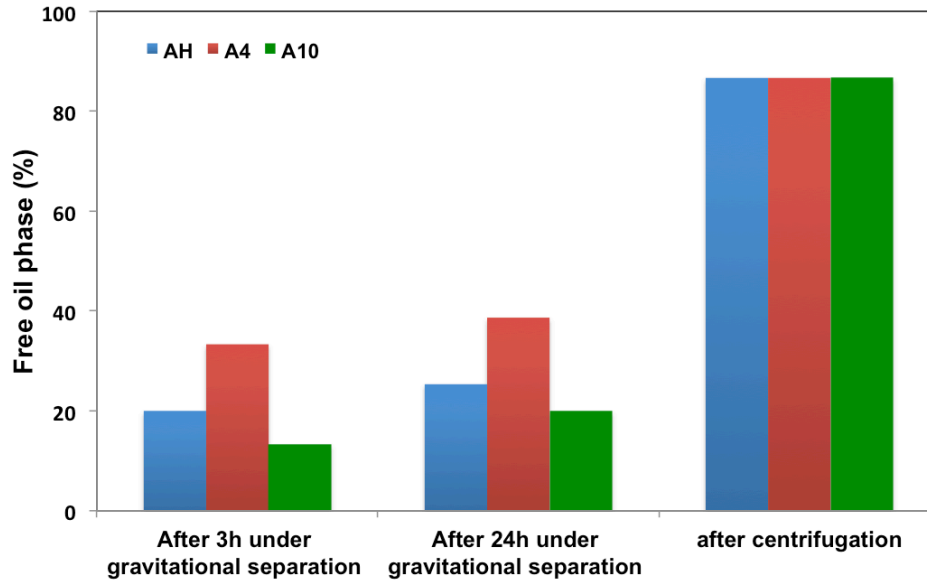
377

### 378 **3.4 Emulsion Stability**

379 Emulsions were prepared with a 60:40 ratio of heptane/toluene because this  
 380 heptol composition is beyond the precipitation onset point for all subfractions. A  
 381 water percentage of 50% was selected to obtain a sufficient volume of emulsion.

382 The stability of asphaltenes emulsions was evaluated through the water and oil  
 383 resolution during 24h under gravitational forces. **Figure 8** shows the separation phase  
 384 evolutions. After 3h under gravitational separation, a free oil layer was observed at  
 385 the top of the centrifugation tube for all emulsions. However, the free oil amount of  
 386 the emulsion synthesized with subfraction A10 was smaller, showing that this  
 387 subfraction has been more efficient in stabilizing emulsions (Zaki *et al.*, 2000). In the  
 388 period from 3h up to 24 h, all emulsions remained stable, no distinguishable water  
 389 phase was observed and free oil phase remained practically the same.

390



391

392 **Figure 8.** Phase separation evolution of model water-in-oil emulsions involving  
 393 subfractions AH, A4 and A10.

394

395 After gravitational separation, to accelerate the process of destabilization, the  
 396 emulsions were centrifuged at 5000rpm for 15 min. **Figure 9** shows the image of the  
 397 system after centrifugation. The centrifugal forces were insufficient to separate the  
 398 water in the emulsions containing the asphaltenes subfractions AH, A4 and A10. On  
 399 the other hand, the separated oil phase increased significantly. It can be observed that  
 400 the droplets settled forming a dense packed layer. The DLPs formation can reduce the  
 401 emulsion separation efficiency (Kelesoglu *et al.*, 2014) because portions of the oil  
 402 remain dissolved in the aqueous phase. All the DLPs formed remained stable for more  
 403 than 2 weeks.

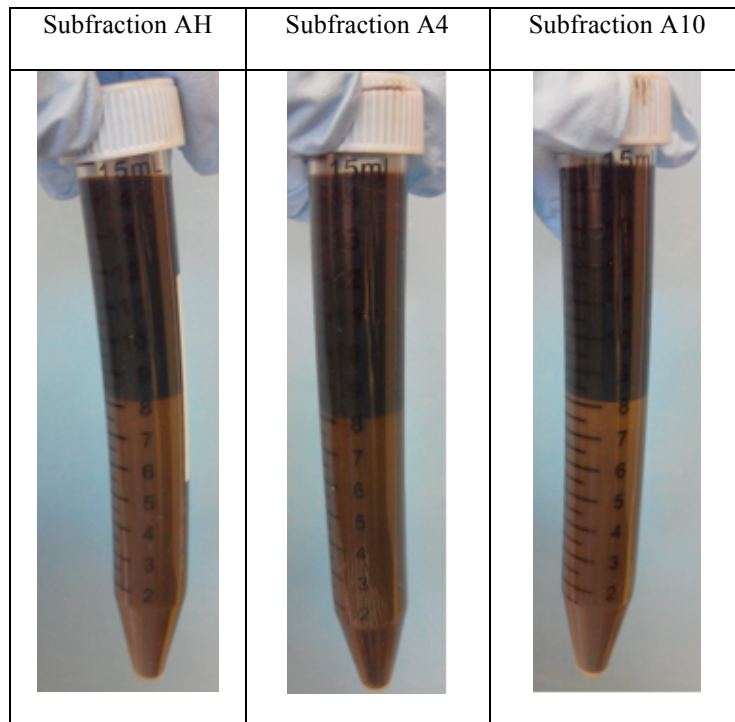
404

405

406

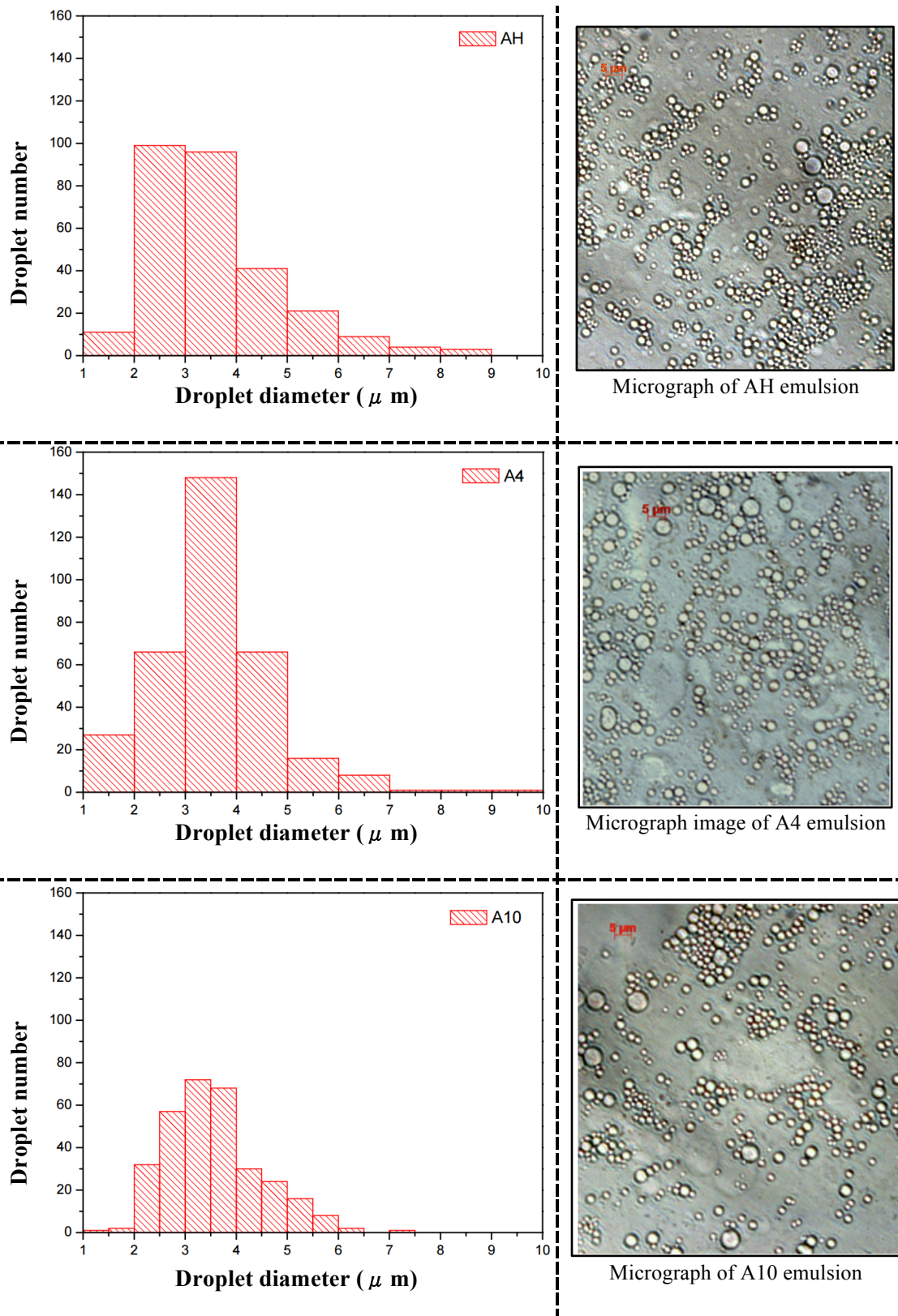
407

408



409 **Figure 9.** Centrifugation results of model water-in-oil emulsions involving  
 410 subfractions AH, A4 and A10.

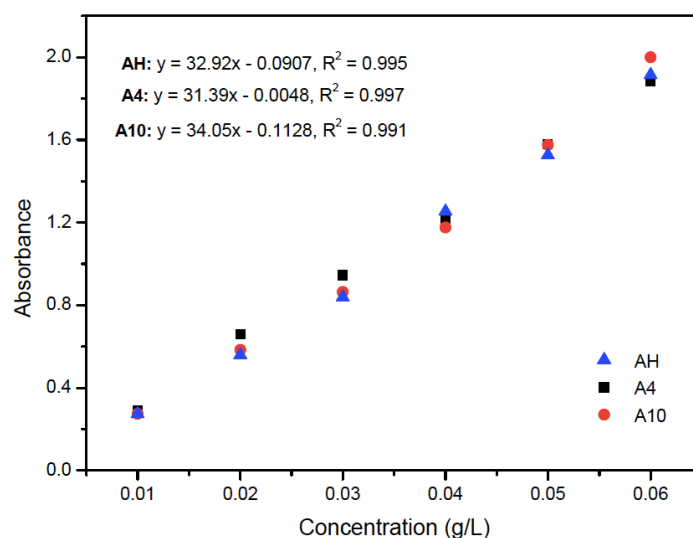
411  
 412 **Figure 10** shows the droplet size distribution generated from the micrographs  
 413 obtained 24 h after the emulsification using an inverted microscopy. The droplet sizes  
 414 varied between 2  $\mu\text{m}$  and 6  $\mu\text{m}$  for all samples. However, the droplets of the  
 415 emulsions stabilized with the subfractions AH and A10 had value well distributed on  
 416 this range and droplets in the emulsion stabilized with the A4 subfraction had  
 417 diameters more concentrated in the range 3–4  $\mu\text{m}$ . The average droplet size were  
 418 very similar, approximately  $d = 3.27\mu\text{m}$  to subfraction AH;  $d = 3.52 \mu\text{m}$  to  
 419 subfraction A4 and  $d = 3.49$  to subfraction A10.



420 **Figure 10.** Histograms of the droplet size distribution generated through of the  
 421 micrographs obtained 24 h after the emulsification using an inverted microscopy.

422

423 | **Figure 11** shows the calibration curve of solutions of the subfraction AH,  
 424 subfraction A4 and subfraction A10 in toluene at concentrations ranging from 0.01 to  
 425 0.06 g.L<sup>-1</sup>, for which UV-visible calibration curves were built at 336nm. It is possible  
 426 to observe a perfect linear dependence of absorbance with concentration. Based on the  
 427 linear regression of the absorbance-concentration data for each subfraction, it was  
 428 possible to evaluate the final concentration of the asphaltene subfractions adsorbed on  
 429 DLP.  
 430



431  
 432 **Figure 11.** Calibration curves of solutions of subfraction AH, A4 and A10 in toluene.  
 433

434 **Table 2** compares the initial concentration of asphaltenes in the oil phase,  
 435 asphaltene concentration in the oil phase after centrifugation and the water content in  
 436 the DLP. The adsorbed amount of the asphaltene A4 in the DLP was the higher,  
 437 approximately 54%, however, a lower percentage of water was observed among all  
 438 samples. Is most likely driven by polar interactions, the A4 subfraction migrated  
 439 preferentially to the aqueous phase destabilizing the DLP. The subfraction A10  
 440 showed higher efficiency in the stabilization of the emulsion. Due aromaticity, the  
 441 A10 subfraction migrated in more quantity to the oil phase, even with lowest

442 concentration adsorbed on DLP, approximately 48%, A10 was able to keep the model  
443 emulsions stable containing more than 87% of water.

444

445 **Table 2.** Concentration of asphaltene subfractions AH, A4 and A10 in the oil phase  
446 after centrifugation and the water content in the DLP formed

	Conc. of asphaltene in oil phase (g.L <sup>-1</sup> )	Conc. of asphaltene in oil phase after separation of DLP (g.L <sup>-1</sup> )	% Water in DLP
Subfraction AH	5.0	2.6 ± 0.1	87 - 90%
Subfraction A4	5.0	2.3 ± 0.2	85 - 87%
Subfraction A10	5.0	2.9 ± 0.1	87 - 89%

447

#### 448 **4. Conclusion**

449 Asphaltenes were extracted from a Brazilian vacuum residue by two different  
450 methods. The whole asphaltene was precipitated with excess of *n*-heptane at the ratio  
451 of 40:1 (*n*-heptane/VR). The subfraction obtained from this first precipitation called  
452 AH, represented 11.2wt%. In the second stage, two successive precipitations were  
453 made based on the ratio of *n*-heptane/VR 4:1 and 10:1, obtaining two different  
454 subfractions of asphaltenes, A4 and A10, which yields 6.8 wt% and 3.1wt%,  
455 respectively. The precipitation in stages proved to be very effective; with an addition  
456 about 40% less solvent, 89% of all asphaltenes present in the vacuum residue were  
457 recovered.

458 Important parameters of the three subfractions as: polarity, aromaticity,  
459 chemical composition and molecular weight were obtained through the analytical  
460 technique of APPI(+)-FT-ICR MS and NMR. The analysis of APPI(+)-FT-ICR MS  
461 showed similarities between the AH and the subfraction A10. The A4 subfraction



462 showed a higher molecular weight distribution and a higher percentage of nitrogen  
463 compounds, being the most polar asphaltene subfraction among them. However the  
464 data show that whole asphaltene AH and sub subfraction A10 involved higher  
465 aromaticity and solubility in *n*-heptane/toluene solutions.

466         The properties of the model emulsions with the different subfractions, such as  
467 water content, droplet size distribution and gravitational separation, showed that the  
468 effect of the whole asphaltene AH, A4 and A10 subfractions in the stability were  
469 generally similar, with all subfractions stabilizing the emulsions for more than two  
470 weeks and without the presence of a free water layer during that entire period.  
471 However, subfraction A10 was the one that maintained a higher percentage of stable  
472 water in the DLP with a lower concentration, in addition to presenting a better  
473 distribution in droplet size and a smaller separation of phase oil during the 24 hours  
474 on gravity action. These results suggest that the aromaticity and lowest molar mass of  
475 subfraction A10 contributed to their self-association this may reflect in a more rigid  
476 interfacial film formation responsible for the DLP more stable. This research also  
477 suggests that subfractions of asphaltene molecules are so effective as the "whole"  
478 fraction in emulsion stability.

479

#### 480 **Acknowledgments**

481         Portions of this work were carried out as a part of the Joint Industrial  
482 Programme (JIP) Asphaltenes consortium “Improved Mechanisms of Asphaltene  
483 Deposition and Precipitation to Minimize Irregularities in Production and Transport –  
484 A Cost Effective and Friendly Approach sponsored by the Norwegian Research  
485 Council (234112/E30) and the following industrial sponsors: AkzoNobel, BP, Canada  
486 Natural Resources, Nalco Champion, Petrobras, Statoil and Total. Thanks are also due

487 to FAPES (73309516/2016), PETROBRAS, CNPq, and CAPES(23038.007083/2014-  
488 40) for their financial support.

489

#### 490 **References**

491 Acevedo, S.,Guzman, K.;Ocanto, O., 2010.Determination of the number  
492 averagemolecular mass of asphaltenes (Mn) using their soluble A2 fraction and  
493 thevapor pressure osmometry (VPO) technique, Energy& Fuels. 24, 1809–1812.

494 Al-Sahhaf, T., Elsharkawy, A.,Fahim, M., 2008.Stability of Water-in-Crude Oil  
495 Emulsions: Effect of OilAromaticity, Resins to Asphaltene Ratio, and pH of  
496 Water. Petroleum Science and Technology. 26, 2009-2022.

497 Castillo, J.,Ranaudo, M. A., Fernández, A., Piscitelli, V., Maza, M., Navarro, A.,  
498 2013. Study of the aggregation and adsorption of asphaltene sub-fractions A1 and A2  
499 by white light interferometry: Importance of A1 sub-fraction in the aggregation  
500 process. Colloids and Surfaces A: Physicochemical and Engineering Aspects. 427,  
501 41-46.

502 Cho, Y., Na, J. G.,Nho, N. S., Kim, SH., Kim, S., 2012. Application of Saturates,  
503 Aromatics, Resins, and Asphaltenes Crude Oil Fractionation for Detailed Chemical  
504 Characterization of Heavy Crude Oils by Fourier Transform Ion Cyclotron Resonance  
505 Mass Spectrometry Equipped with Atmospheric Pressure Photoionization. Energy  
506 &Fuels. 26, 2558-2565.

507 Da Silva Oliveira, E. C., Neto, Á. C., Júnior, V. L., de Castro, E. V. R., De Menezes,  
508 S. M. C., 2014.Study of Brazilian asphaltene aggregation by Nuclear Magnetic  
509 Resonance spectroscopy.Fuel.117, 146-151.

510 Dudásova, D., Simon, S., Hemmingsen, P. V., Sjoblom, J., 2008. Study of asphaltenes  
511 adsorption onto different minerals and clays Part 1. Experimental adsorption with UV  
512 depletion detection. *Colloids and Surfaces*. 317, 1-9.

513 Fossen, M., Sjoblom, J., Kallevik, H., Jacobsson, J., 2007. A New Procedure for Direct  
514 Precipitation and Fractionation of Asphaltenes from Crude Oil. *Journal of Petroleum  
515 Science and Technology*. 28, 193-197.

516 Kendrick, E., 1963. A Mass Scale Based on  $CH_2 = 14.0000$  for High Resolution  
517 Mass Spectrometry of Organic Compounds. *Analytical Chemistry*. 35, 13, 2146-  
518 2154.

519 Klein, G. C., Kim, S., Rodgers, R. P., Marchall, A. G., 2006a. Mass Spectral Analysis  
520 of Asphaltenes. II. Detailed Compositional Comparison of Asphaltenes Deposit to Its  
521 Crude Oil Countepart for Two Geographically Different Crude Oils by ESI FT-ICR  
522 MS. *Energy & Fuels*. 20, 1973 – 1979.

523 Klein, G. C., Kim, S., Rodgers, R. P., Marshall, A. G., 2006b. Mass Spectral Analysis  
524 of Asphaltenes. I. Compositional Differences between Pressure-Drop and Solvent-  
525 Drop Asphaltene Determined by Electrospray Ionization Fourier Transform Ion  
526 Cyclotron Resonance Mass Spectrometry. *Energy & Fuels*. 20, 1965 – 1972.

527 Loureiro, T., Palermo, L., Spinelli, L., 2015. Influence of precipitation conditions (n-  
528 heptane or carbon dioxide gas) on the performance of asphaltene stabilizers. *Journal  
529 of Petroleum Science and Engineering*. 127, 109-114.

530 Nalwaya, V., Tantayakom, V., Piumsomboon, P., Fogler, S., 1999. Studies on  
531 Asphaltenes through Analysis of Polar Fractions. *Industrial & Engineering Chemistry  
532 Research*. 38, 3, 964-972.

533 Nascimento, P. T. H., Santos, A. F., Yamamoto, C. I., Tose, L. V., Barros, E. V.,  
534 Gonçalves, G. R., Freitas, J. C. C., Vaz, B. G., Romão, W., Scheer, A. P., 2016.

535 Fractionation of Asphaltene by Adsorption onto Silica and  
536 Chemical Characterization by Atmospheric Pressure Photoionization Fourier  
537 Transform Ion Cyclotron Resonance Mass Spectrometry, Fourier Transform Infrared  
538 Spectroscopy Coupled to Attenuated Total Reflectance, and Proton Nuclear Magnetic  
539 Resonance. *Energy & Fuels*. 30, 5439-5448.

540 Pereira, T.M.C., Vanini, G., Oliveira, E.C.S., Cardoso, F.M.R., Fleming, F.P., Neto,  
541 A.C., Lacerda Jr., V., Castro, E.V.R., Vaz, B. G., Romão, W., 2014a. An evaluation of  
542 the aromaticity of asphaltenes using atmospheric pressure photoionization Fourier  
543 transform ion cyclotron resonance mass spectrometry – APPI(±)FT-ICR MS. *Fuel*.  
544 118, 348-357.

545 Pereira, T. M. C., Vanini, G., Tose, L. V., Cardoso, F. M. R., Fleming, F.P., Rosa, P.  
546 T. V., Thompson, C. J., Castro, E. V. R., Vaz, B. G., Romão, W., 2014b. FT-ICR MS  
547 analysis of asphaltenes: Asphaltenes go in, fullerenes come out. *Fuel*. 131, 49-58.

548 Rogel, E., Roye, M., Vien, J., Miao, T., 2015. Characterization of Asphaltene  
549 Fractions: Distribution, Chemical Characteristics, and Solubility Behavior. *Energy*  
550 *& Fuels*. 29, 4, 2143-2152.

551 Samaniuk, J., Hermans, E., Verwijlen, T., Pauchard, V., Vermant, J., 2015. Soft-Glassy  
552 Rheology of Asphaltenes at Liquid Interfaces. *Journal of Dispersion Science and*  
553 *Technology*. 36, 10, 1444-1451.

554 Sjoblom, J., Aske, N., Auflen, I. H., Brandal, O., Havre, T. E., Saether, O., Westvik,  
555 A., Johnsen, E. E., Kallevik, H., 2003. Our Current Understanding of Water-in- Crude  
556 Oil Emulsions. Recent Characterization Techniques and High Pressure  
557 Performance. *Advances in Colloid and Interface Science*. 100, 102, 399-473.

558 Sjoblom, J., Simon, S.; Xu, Z., 2015. Model molecules mimicking asphaltenes,  
559 *Advances in Colloid and Interface Science*. 218, 1-16.

560 Speight, J.G., 2007. The Chemistry and Technology of Petroleum, 4ed., New York.

561 Spiecker, P. M., Gawrys, K. L., Kilpatrick, P. K., 2003. Aggregation and solubility  
562 behavior of asphaltenes and their subfractions. Journal of Colloid and Interface  
563 Science. 267, 178-193.

564 Trejo, F., Centeno, G., Ancheyta, J., 2004. Precipitation, fractionation and  
565 characterization of asphaltenes from heavy and light crude oils. Fuel. 83, 16, 2169-  
566 2175.

567 Van Krevelen, D. W., 1950. Graphical statistical method for the study of structure and  
568 reaction processes of coal. Fuel. 29, 269-84.

569 Zaki, N., Schorring, P.-C., Rahimian, I., 2000. Effect of asphaltene and resins on the  
570 stability of water-in-waxy oil emulsions. Petroleum Science & Technology. 18, 7-8,  
571 945-963.

572 Yang, X., Hamza, H., Czarnecki, J., 2004. Investigation of Subfractions of Athabasca  
573 Asphaltenes and their Role in Emulsion Stability. Energy & Fuels. 18, 770-777.

574 Yang, X., Verruto, V., Kilpatrick, P., 2007. Dynamic Asphaltene-Resin Exchange at  
575 the Oil/Water Interface: Time-Dependent W/O Emulsion Stability for  
576 Asphaltene/Resin Model Oils. Energy & Fuels, 21, 3, 1343-1349.

577